INVESTIGATION OF THE ARCJET NEAR FIELD PLUME USING ELECTROSTATIC PROBES

John M. Sankovic
National Aeronautics and Space Administration
Lewis Research Center
Cleveland, Ohio 44135

ABSTRACT

The near field plume of a 1 kW class arcjet thruster was investigated using electrostatic probes of various geometries. The electron number densities and temperatures were determined in a simulated hydrazine plume at axial distances between 3 cm (1.2 in) and 15 cm (5.9 in) and radial distances extending to 10 cm (3.9 in) off centerline. Values of electron number densities obtained using cylindrical and spherical probes of different geometries agreed very well. The electron density on centerline followed a source flow approximation for axial distances as near as 3 cm (1.2 in) from the nozzle exit plane. The model agreed well with previously obtained data in the far field. The effects of propellant mass flow rate and input power level were also studied. Cylindrical probes were used to obtain ion streamlines by changing the probe orientation with respect to the flow. The effects of electrical configuration on the plasma characteristics of the plume were also investigated by using a segmented anode/nozzle thruster. The results showed that the electrical configuration in the nozzle affected the distribution of electrons in the plume.

INTRODUCTION

The arcjet thruster is an electrothermal propulsion device in which an electric arc is used to heat the propellant. The heated propellant is then converted to directed kinetic energy by expansion of the heated propellant through a Laval nozzle.

Early research in arcjet technology for power levels ranging from 1 to 200 kW was performed in the 1950's through the mid 1960's, and a summary of that research effort was provided by Wallner and Czika[1]. Most of that research centered on the 30 kW power level for planetary applications and demonstrated that the arcjet was capable of providing high specific impulse levels over a wide range of input power. At that time, the lack of an adequate space power source hampered the future application of the arcjet and research ceased.

Because of the high specific impulse the 1 kW class arcjet can offer over existing chemical and resistojet technology, interest in the arcjet has recently increased. The use of the arcjet for north-south stationkeeping (NSSK) can result in significant fuel savings. The resultant mission life extension is estimated to exceed five years for a 1600 kg satellite in geosynchronous orbit[2].

Currently, a 1 kW hydrazine arcjet propulsion system including the power processing unit (PPU) is under development[3]. Performance goals of 450 s specific impulse and lifetimes exceeding 1000 h and 500 cycles have been demonstrated[4]. As the arcjet nears flight readiness, concern is shifting toward spacecraft integration issues.

Two such issues are electromagnetic interference (EMI) generated by the arcjet system[5] and the impact of the exhausted plume on the communications signal and spacecraft surfaces. Experimental studies have been conducted by Carney[6,7] using electrostatic probes to analyze the arcjet exhaust plasma. With the plasma characteristics obtained in those studies, models of the effect of the plume on communications signals have been developed[8,9]. The modeling effort is heavily dependent on a database of plume characteristics for various thruster operating conditions. The first goal of this experimental study was to increase that data base.

Concurrently, research into the physical processes governing the operation of the arcjet is underway. Zube[10], using emission spectroscopic techniques, determined excitation, rotational, and vibrational temperatures as well as electron number densities inside the nozzle. Near the nozzle exit plane, Manzella[11] determined similar quantities and obtained insight into the energy loss mechanisms in the 1 kW class arcjet. The second goal of this work was to provide information to aid in the understanding of the operation of the arcjet.

This study reports the plasma properties in the near field of the 1 kW class laboratory model arcjet. Electron number densities were obtained using electrostatic probes of various geometries and the results are compared. Ion streamlines were obtained in the near field plume using cylindrical probes. The source flow approximation, i.e. the centerline electron number density being inversely related to the square of the axial distance, was investigated in the region less than 15 cm (5.9 in) from the nozzle exit plane. The effects of propellant mass flow rate and power on the electron number density are reported for various axial locations on centerline. Finally, using a segmented anode/nozzle thruster, the impacts of electrical configuration on the plasma properties in the plume were examined.

Approved for public release; distribution is unlimited.

NOMENCLATURE

A	area, m^2
D	probe diameter, cm
e	electron charge, C
I	current, A
I_o	saturation current, A
k	Boltzmann constant, J/K
L	probe length, cm
m	mass, kg
n	number density, particles/m^3
R	probe radius, cm
T	temperature, K
V	potential, V
x	axial distance from nozzle exit, cm
λ_d	Debye length, cm

SUBSCRIPTS:

e	electron
p	probe
∞	plasma

THEORY

The electrostatic or Langmuir probe is a diagnostic technique commonly used for obtaining electron number densities and temperatures in a plasma. An electrostatic probe is basically a small electrode inserted into the plasma and connected to a power supply capable of varying the voltage of the probe relative to the plasma. By measuring the current collected by the probe at various voltages, a current-voltage (I-V) characteristic can be constructed. The I-V characteristic consists of the ion saturation region, the electron retarding or transition region, and the electron saturation region. Although experimental techniques to obtain the characteristic are relatively simple, the theory behind the analysis is quite complex. Carney and Sankovic[7] presented a summary of references for previous Langmuir probe work. Reviews of Langmuir probe theory have been provided by Chen[12], Chung et al[13], and Swift and Schwar[14]. In addition to those works, Laframboise[15] developed a theory for cylindrical and spherical probes in a stationary, collisionless plasma, and experimental work on flowing plasmas was presented by Clayden[16] and Sonin[17].

The analysis of the characteristics is simplified greatly if the electrons are assumed to have a Maxwellian velocity distribution, the plasma is considered collisionless, and the sheath thickness is thin. Under these conditions the electron current collected by the probe can be expressed as:

$$I_e = A_p e n_e \sqrt{\frac{kT_e}{2\pi m_e}} \left\{ \exp\left[\frac{-e\left(V_p - V_\infty\right)}{kT_e} \right] \right\} \qquad (1)$$

The electron temperature is determined by taking the logarithm of Eq. 1 and then differentiating with respect to the voltage of the probe. This results in the following relationship:

$$\frac{d}{dV} \ln\left(I_e\right) = -\frac{e}{kT_e} \qquad (2)$$

The slope of the semi-logarithmic plot of the transition region is therefore inversely proportional to the electron temperature. Assuming the previously stated conditions, the electron saturation current can be expressed as:

$$I_{oe} = A_p e n_e \sqrt{\frac{kT_e}{2\pi m_e}} \qquad (3)$$

Eq. 3 can be solved for the electron number density with the only variables being the electron temperature, the saturation current, and the probe current collecting area. The temperature can be determined from the slope in the transition region. A common technique used to obtain the saturation current from the semi-logrithmic plot of the current-voltage characteristic is to fit straight lines through the transition and the electron acceleration regions. The current at the point of intersection yields the saturation current and the plasma potential. The only unknown which remains is the probe current collection area.

Caution must be used in defining the probe current collecting area. For cylindrical probes, end effects can be ignored if the probe length to diameter (L/D) ratio is large. For spherical probes, the problem is more complicated. Many investigators use the actual surface area, but the validity of this has not be thoroughly demonstrated. Clayden[16]

used a "wetted" surface area which consisted of one-half the actual surface area. His explanation for this was that a wake was formed behind the probe causing an ion void and, due to ambipolar diffusion, a resultant electron void. In a preliminary investigation of wake effects in a arcjet plume, Sankovic and Jankovsky[18] found that the current collecting area did in fact vary between 55 and 75 percent of the actual area. In this study the actual surface area was used in all calculations; the rationale for this is presented in the Results and Discussion section.

By observing the response of a cylindrical electrostatic probe at different angles of incidence, ion streamlines can be determined. Jakubowski[19] has investigated the probe response in a low density hypersonic argon plasma and found that over the range $0.5 \leq R_p/\lambda_d \leq 2$, the ion current collected by the probe is a strong function of the ratio of probe radius to Debye length. For that entire range at a zero angle of attack, a maximum or relative maximum occurs in the ion current. By placing a probe at any location in the plume and simultaneously collecting current while rotating the probe, the flow direction is determined by the angle at which this relative maximum occurs.

EXPERIMENTAL APPARATUS

LANGMUIR PROBES

Previous studies of the arcjet plume[6,7] dealt with the far field where the plasma parameters do not change as rapidly with position as in the near field, and the geometry of the probe could be kept constant over large spatial regions. In the region within 15 cm (5.9 in) of the thruster, the area of concern in this report, the electron number density can change by orders of magnitude over a few centimeters, and a single probe geometry may only be appropriate for a small region. To facilitate the use of probes of varying geometry and to minimize the perturbations to the flow by the probe, a new probe design was developed and tested.

The new design was modular and allowed the reuse of the probe support. The cylindrical probe shown in Fig. 1 consists of a tungsten wire which was either 0.0076 cm (0.003 in) or 0.013 cm (0.005 in) in diameter and of various lengths. The tungsten wire was copper plated at one end and soldered to a male pin connector. The wire was isolated from the plasma by a quartz capillary tube of 0.025 cm (0.010 in) internal diameter inside a piece of alumina. A second piece of alumina with an internal diameter equal to the outer diameter of the other alumina section and the pin connector served as the final electrically isolating section. A high temperature ceramic adhesive was used to bond the two alumina sections together. The entire assembly was inserted in a hollowed stainless steel bolt and fastened by a set screw. The bolt allows attachment of the probe to the support structure.

The spherical probes were of the same basic design as their cylindrical counterparts except that a metal sphere consisting of a steel bearing ball with a 0.025 cm (0.010 in) hole extending half the diameter into the sphere was brazed onto the tungsten wire. The weakness of this design was the braze joint which limited the temperatures the probe could endure.

The probe support structure with a spherical probe is shown in Fig. 2, and consisted of a stainless steel tube bent at a 90° angle and tapped to match the thread of the probe assembly bolt. On the other end was a bulkhead fluid fitting, attached to a small aluminum box with a BNC connector. Electrical continuity with the probe was accomplished through the use of a copper wire encased in a fiberglass sheath inside the stainless steel tubing with one end attached to the center of the BNC and the other to a female pin connector.

For flow angle studies, the cylindrical probe must rotate about its center. Coarse alignment was provided by an aluminum bar attached to the bottom of the probe support and then to the rotary actuator. Fine alignment was accomplished by loosening the set screw and sliding the probe assembly inside the bolt.

In addition to the single probes, a rake of three probes of similar design was also employed in the experiment. The advantage of the rake was that the vacuum facility did not need to be cycled to change probe geometry.

ARCJET THRUSTER

Two experimental 1 kW class arcjets were used in this study. Thruster A was of a constricted-arc, vortex-stabilized, modular design,[4, 21] which has demonstrated lifetimes over 1000 h. Thruster B employed a segmented anode/nozzle and was the thruster used by Curran[20] and Manzella[11].

In both thrusters, the anode served as the nozzle and consisted of a converging side with a conical geometry and half angle of 30°, the constrictor, and a diverging side with a conical half angle of 20°. The only difference between the two thrusters was the segmentation of the diverging side of the Thruster B anode/nozzle; otherwise, the geometry of the nozzles of both thrusters was the same. Each nozzle had an area ratio of 225 and a constrictor diameter of 0.0635 cm (0.025 in). The nozzle of Thruster A was fabricated from a solid piece of 2% thoriated tungsten, and the

nozzle of Thruster B consisted of both isolating segments of boron nitride and conducting segments of 2% thoriated tungsten and tantalum, respectively. Fig. 3 shows a schematic representation of the segmented anode.

The arcjet cathode was fabricated from a 0.318 cm (0.125 in) diameter 2% thoriated tungsten welding rod, one end of which was tapered to a 30° half angle. The cathode was isolated from the anode through the use of boron nitride insulators. The cathode was anchored, and the arc gap is set , using a modified fluid fitting and a ferrule. The arc gap[21] was set at 0.058 cm (0.023 in).

ARCJET POWER PROCESSOR

The power electronics for the start-up and steady state operation of the arcjet have been decribed in detail by Gruber[22]. In summary, the arcjet power converter was pulse-width modulated and closed-loop configured to give fast current control. Instantaneous current control and the high voltage pulse for arc ignition were provided by an inductor in series with the arcjet. The power processor was capable of delivering 11 A with up to 140 Vdc to the arcjet. The high voltage pulse used for arc ignition was nominally 3 kV.

POSITIONING SYSTEM

A picture of the positioning system is presented in Fig. 4. The system consisted of one rotary and four linear actuators, which were powered by 200/400 step per revolution stepper motors. The actuators were direct-driven reciprocating ball type with a pitch of 2 revolutions per centimeter and a travel of 30.5 cm (12 in) Two of the actuators were used for arcjet positioning while the remaining three were used for probe positioning. A probe was able to be positioned to radial distances extending to 15 cm (5.9 in) on both sides of plume centerline. Axial distances of over 50 cm (19.7 in) could be achieved and full 360° rotation was possible. All actuators were mounted on an aluminum frame which allowed facile removal of the entire assembly from the vacuum facility. While in the vacuum chamber, the system was mounted on rubber elastomer vibration mounts to minimize the transmission of the facility vibrations to the probe. By having the arcjet and probe actuators mounted on the same frame, no vibration problems were experienced. Position increments as small as 0.05 mm (0.002 in) have been used repeatably and, due to the use of stepper motors, the uncertainty in positioning was not cumulative.

VACUUM FACILITY

All data were taken in the Tank 8 Space Environment Facility at the NASA Lewis Research Center. The facility is a 1.5 m (5 ft) diameter by 5 m (16 ft) long cylindrical vacuum vessel, equipped with four 0.82 m (2.7 ft) diameter oil diffusion pumps, each with a pumping capacity of approximately 14,000 lps at 0.013 Pa (1 x 10^{-4} torr). The diffusion pumps are backed by a rotary blower and two mechanical rough pumps. The pressure during all experiments was below 0.067 Pa (5 x 10^{-4} torr).

PROBE ELECTRONICS AND DATA ACQUISITION

A schematic of the experimental setup is presented in Fig. 5. The bias on the probe was supplied by a bipolar power supply capable of supplying ±100 V at 1 A. The power supply was driven by an external source and output 5 times the input voltage. A programmable function generator inputting a sawtooth waveform into the bipolar supply was used to create the necessary voltage ramp. The advantage of this method was that only commercially available components were necessary, and varying the sweep rate was a simple task.

Low inductance resistors were used in the system to provide a method of probe current measurement. Hall-effect current probes were tried, but the zero drift with time was too large in comparision to the signal. The voltage drop across the resistors was measured using a commercially available differential amplifier with selectable filters. The filters were necessary because the arcjet power processing unit provides current to the arcjet with an a.c. frequency component of approximately 10 kHz. This ripple could affect the plasma plume and caused a large scatter in the probe characteristic data if a filter was not used.

The output of the amplifier and probe voltage sensing leads were input to a 1 MHz four channel multiplexed data acquisition board with 12 bit resolution installed in a microcomputer using 20 MHz 80386 and 80387 microprocessors. The computer also controlled the movement of the three probe positioning actuators inside the vacuum facility. The arcjet positioning actuators were controlled by a separate microcomputer used for spectroscopic studies. A high precision electrometer was used to measure the ion current for the ion streamline studies.

EXPERIMENTAL PROCEDURE

LANGMUIR PROBE

The probe was ramped from ±5 V at a frequency of 1 Hz. Previous work[7] indicated that the 10 V range was sufficient to capture both the electron and ion saturation regions. The effects of sweep rate (i.e. probe capacitance) were investigated briefly. Using a digital oscillosope, the current signal was observed for sweep rates of 1, 10, 100, and 1000 Hz. Slight degradation of the I-V characteristic began to appear at 100 Hz, and degradation was very pronounced at 1 kHz.

The effects of the input filtering on the differential amplifier used to measure the current were also investigated. I-V characteristics were taken using a ±5V ramp at 1 Hz and a selection of 0.1 kHz, 0.3kHz, 1kHz, and 10kHz filters. The data were analyzed, and the resultant values of electron number density and temperature were in good agreement. The sample rate of the data acquisition system was 1 kHz and 1000 data points were taken. The 0.1 kHz filter minimized the large amplitude oscillations in the I-V characteristic observed in previous studies[7].

The issue of probe cleaning was also addressed. Two methods are frequently employed, and both suffer from disadvantages. For electron emission the probes are heated to a very high temperature and may be damaged. On the other hand, ion sputtering can contaminate insulating sections of the probe, making them conductive. For this study, the probes were cleaned by electron emission, because of the advantage of being able to visually monitor the heating of the probe. The probes were manually biased to +100 V at approximately 10 cm (3.9 in) on centerline of the plume and then the voltage was immediately reduced. This was quite sufficient to make the probe glow very brightly. No change in the characteristic occured if this procedure was repeated; therefore, it was concluded that one cycle was sufficient for probe decontamination. At the high temperatures encountered in the near field, susceptibility to contamination was minimized.

The data reduction scheme used a least squares algorithm to fit a line through the ion saturation region. The line was extrapolated and the ion contribution along with any zero offset was subtracted from the total current trace to obtain the electron current. Again using the least squares routine, a line was fitted through the electron retarding region and through the electron acceleration region. The end points of the fit were selected interactively by the user. The inverse of the slope of the line through the transition region gave the electron temperature and the intersection of the line through the transition region and the electron saturation region gave the plasma potential and the saturation current from which the electron number density was calculated.

The uncertainty in the electron temperature measurements increased as the axial distance increased, due to a decrease in the current collected by the probe, but was always less than ±0.05 eV. Using the square root of the sum of the squares of the uncertainties in the probe area, electron temperature, and saturation current, a worst case uncertainty in the electron number densities was determined to be 20%; however, for the majority of data, the uncertainty was much less. All probe positions reported were measured from the center of the probe. Uncertainty in probe alignment between runs was less than ±0.25 mm (0.010 in).

ARCJET THRUSTER

Thruster A was used for all the studies excluding the electrical configuration work, which utilized Thruster B. Thruster A had been used in previous experiments and had several hundred hours of accumulated run time since its last assembly, and it was not disassembled at any time throughout the experiment. As mentioned previously, Thruster B was the same segmented anode thruster used by both Curran[20] and Manzella[11]. The operating procedure for that thruster is discussed at length in Reference 20. Before any data were taken, both thrusters were allowed to reach thermal and electrical equilibrium. This required approximately thirty minutes from a cold start and fifteen minutes from an operating parameter change.

The arcjet current was measured using a Hall-effect current probe which was calibrated before each run. The arcjet voltage was measured at the anode and cathode leads entering the vacuum facility using a digital multimeter. The propellant in all cases was a simulated hydrazine mixture of hydrogen and nitrogen in a 2:1 ratio by volume. The propellant flow rate was measured using thermal conductivity-type flow meters with 5.00 SLPM full scale readings. The flow meters were calibrated as discussed in Reference 20. The calibration was repeated several times throughout this study, and the fluctuation between calibrations was typically 1% or less.

RESULTS AND DISCUSSION

PROBE GEOMETRIES

Plume characteristics were taken using cylindrical probes with three different geometries to study the effects of the probe L/D ratio. The L/D ratios tested were 52, 80, and 130. Data were taken on the plume centerline at axial distances of 3.2 cm and 15.5 cm for Thruster A operating at 10 A and 115 V with a propellant flow rate of 49 mg/s. The electron number densities and electron temperatures obtained are presented in Figs. 6 and 7, respectively. Figures 6 and 7 show excellent agreement between electron number densities and temperatures obtained for all three probe geometries. Data from two separate runs, taken using the same probe, are also shown in Figs 6 and 7 to illustrate the repeatability from test to test. The electron temperatures ranged between 0.15 eV and 0.3 eV. Any trend in the electron temperature is masked by the scatter. In general the data between all three geometries are in agreement and the electron temperature appears constant over the axial distances evaluated.

Figure 8 shows a plot of the electron number density obtained using a 130 L/D, 0.0076 cm (0.003 in) diameter cylindrical probe and a 0.32 cm (0.125 in) diameter spherical probe. Thruster A was used under the same operating conditions stated previously. The Rp/λ_d ratio ranged between 53 and 94 for the spherical data and between 1.5 and 3.8 for the cylindrical data. Because of the excellent agreement with cylindrical probe results, the actual surface area was used as the current collecting area for the spherical probes. Carney and Sankovic[7] found it necessary to use a correction factor of 0.7 to account for wake effects with spherical probes, but used probes of a much larger diameter. A systematic study is needed to determine at what plasma characteristics and probe geometry wake effects become important.

ION STREAMLINES

Using a cylindrical probe of 0.0076 cm (0.003 in) diameter and a L/D of 130, rotary surveys were obtained and ion streamlines were determined with the arcjet running at 12 A and 110 V with a propellant mass flow rate of 49 mg/s. Two sample surveys are given in Fig. 9. Zero degrees corresponds to the orientation where the probe length is parallel to the thruster centerline. In Fig. 9 the data were taken on centerline and at 2 cm off centerline. For the centerline survey, a relative maximum can be seen at zero degrees, and as the probe is moved off centerline, this maximum shifts corresponding to the ion expansion. Jakubowski[19] found that the variation of the ion current with the probe orientation varied greatly with R_p/λ_d ratio. The R_p/λ_d for the centerline data in Fig. 9 was 1.8 and the shape of the curve agrees well with those shown by Jakubowski[19]. Figure 10 shows the ion streamlines obtained in the near field, and the location of each data survey is marked by an arrow. The data taken at two radial locations closest to the arcjet nozzle exit plane at 1.4 cm (0.55 in) and 2.4 cm (0.94 in), show a rapid ion expansion. At 2.4 cm (0.94 in), the streamline at a radial distance of 2 cm (0.79 in) is 53 degrees and reaches 85 degrees at 6 cm (2.4 in) from the centerline.

Assuming that the neutral particles, which are responsible for the vast majority of momentum transfer, follow the same trajectory as the ions, the data allow qualitative interpretation of the nozzle performance. The 1 kW class arcjet exhaust plume has a very low ionization fraction, and the ion-neutral mean free path is three orders of magnitude less than the ion-electron mean free path; therefore, the ion expansion is not dominated by ambipolar diffusion and is a gas dynamic result[7]. The abrupt turning of the flow may be due to the boundary layer at nozzle lip or simply due to expansion waves. Using Prandtl-Meyer theory and the assumption that the arcjet exhaust is a mixture of N_2 and H_2 at 2000 K which exits the nozzle at 4500 m/s and is turned 65°, the resultant Mach number after expansion is 19. This is an unrealistic result and suggests that the turning of the flow is due to viscous effects in the nozzle. Those effects are a loss mechanism, and reduction of the turning at the lip may lead to optimization of the nozzle.

SOURCE FLOW MODEL

Previous models of the arcjet plume used a source flow approach where the flow field was modeled as an expansion from a point source and the centerline density was a function of the square of the inverse of the distance. A widely used source flow method for the prediction of rocket exhaust plumes has been presented by Simons[23]. Near the nozzle this model should fundamentally break down. Evidence of this can be seen in Fig. 10. The rapid expansion of the ions near the nozzle exit plane does not correspond to a source flow model.

Figure 11 is a plot of the electron number density on plume centerline showing the data of References 7,10 and 11 along with the data obtained in this study. The data presented in this work were obtained with an arcjet operating at 10A and 115 V with a propellant flow rate of 49 mg/s and using a 0.0076 cm (0.003 in) diameter, L/D=100, cylindrical Langmuir probe. The current and referenced data were taken under similar, but not identical, conditions and methods, and it is important to note the difference between the four data sets. The data taken by Zube[10] and Manzella[11] used emission spectroscopic techniques, while this study and that done by Carney and

Sankovic[7] used electrostatic probes. In both this study and in the work by Manzella[11], the same arcjet and operating conditions were used. Zube[10] and Carney and Sankovic[7] used different arcjets of the same nominal design.

An excellent fit to the data was obtained using a linear least squares algorithm on a log-log plot of the data. The electron number density was found to be proportional to the inverse square of the axial distance. When the fit is extrapolated into the far field, the estimate at 32 cm (12.6 in) is slightly higher than that obtained by Carney and Sankovic[7]. One possible explaination for the difference is that two different thrusters were used. The effects of arc gap and cathode and anode geometry are not fully understood; however, it is known that different arcjets have slightly different distributions of electrons in the plume. When the fit is extrapolated in the near field, the model underestimates the results obtained by Manzella[11] and cannot be used inside the nozzle to compare with Zube[10]. At one centimeter downstream of the nozzle exit, the source flow model predicts an electron density of 1.8×10^{12} cm^{-3}. Manzella[11] using emission spectroscopic techniques, determined the value to be 1×10^{13} cm^{-3}. This underestimation indicates a breakdown of the source flow model in the region less than 3 cm from the nozzle exit. The data from all four studies can be represented by a single curve and are in general complementary.

EFFECTS OF POWER LEVEL AND PROPELLANT FLOW RATE

Electron number density contours were obtained for a constant propellant flow rate of 49 mg/s and power levels of 1140 W at 10 A and 940 W at 7.5 A. All data were taken using a 0.32 cm (0.125 in) diameter spherical probe. The contours are shown in Figs. 12 and 13, respectively. Locations where data was obtained are marked in the figures by asterisks. The region consisting of axial distances less than 7 cm (2.8 in) and radial distances less than 2 cm (0.79 in) has been blocked out. Due to the hostile probe environment is this region, no spherical probe data were taken. Extrapolation by the software into that region would not provide accurate results, since the software will not tolerate a discontinuity in the number density, such as the one which occurs at the thruster body/exhaust plume boundary. In both figures the expansion of electrons behind the arcjet is noted; although, the number density is quite low (approximately 2×10^{9} cm^{-3}). As would be expected, higher power levels result in a steeper radial number density gradient. Both exponential and cosine functions, which were used by Simons[23] in his source flow model, were tried and resulted in unsatisfactory fits. This is most probably due to the breakdown of the point source approximation in a region so close to the nozzle exit plane.

Plume data was taken for Thruster A operating at propellant mass flow rates of 45, 40, 35, and 30 mg/s and at current levels of 6, 8, and 10 A at each flow rate. Data were taken on plume centerline at an axial distance of 10.16 cm, using a 0.79 cm (0.125 in) diameter spherical probe. Figures 14 and 15 present the electron number density and temperature data as a fuction of specific power. The electron number density is a strong function of both the propellant mass flow rate and the input current level. For each mass flow rate, higher current levels result in higher electron number densities. Likewise, an increase in mass flow rate at a constant current level causes an increase in the electron number density on centerline. This result is similar to those obtained by Carney and Sankovic[7] at 32 cm (12.6 in). The electron temperature seems to only be a function of the current level as is shown by Fig. 15. As the current decreases, the electron temperature increases. Figures 16 and 17 show the results obtained at a constant power and different mass flow rates. An increase in mass flow rate results in an increase in electron density on centerline. In a free burning arc, the increase in deionizing collisions with an increase in mass flow rate would tend to bring the electron number density down[24]. Clearly, this is not the case in the arcjet. The mass flow rate appears to be a very dominant factor influencing the electron density in the plume, and further discussions on the topic are delayed until the next section on the Effects of Electrical Configuration.

EFFECTS OF ELECTRICAL CONFIGURATION

The segmented anode/nozzle arcjet, Thruster B, was run with four electrical configurations at a total current level of 10 A. The electrical configurations are referred to as 0 through 3, and these are shown in Table I. A 0.0076 cm (0.003 in) diameter cylindrical probe with L/D=100 was used to obtain data on thruster centerline at axial distances ranging between 3 cm (1.2 in) and 9 cm (3.5 in). The electron density data are given in Fig. 18, and the temperature data is presented in Fig. 19. The electron density data appear to be basically unchanged for Configurations 0,1, and 2. In Configuration 3, all current was forced to attach at the farthest downstream nozzle segment, and the electron density on centerline appears significantly higher. Although the scatter in the electron temperature data of Fig. 19 is relatively large, the temperatures associated with Configuration 3 were found to be slightly lower than those observed for the other configurations.

The data presented in Fig. 18 can be used to partially explain the mass flow data presented in the previous section. As the mass flow increases, the upstream chamber pressure increases, and the higher pressure forces the arc attachment farther downstream as shown in Reference 20. From the electrical configuration data, it has been shown that as the arc attachment is forced downstream the centerline electron number density increases; consequently, increased propellant flow rates at constant power levels cause an increase in centerline electron density. Another contribution to the increase in centerline density may be caused by greater constriction of the arc by the higher

pressure[24]. This constriction would cause the centerline enthalpy to increase and thereby increase the number of electrons.

A spherical probe of 0.32 cm (0.125 in) diameter was used to obtain radial data at 14.16 cm (5.6 in) downstream of the Thruster B nozzle exit plane for radial distances extending to 10 cm (3.9 in) from centerline. The data for Configurations 0 and 3 are presented in Fig. 20. Over that range of distances, the distributions do not appear different and the number densities are significantly greater at all locations for the Configuration 3 data.

CONCLUDING REMARKS

Electron density and temperature data have been obtained using electrostatic probes of several geometries in the arcjet plume near field. The results obtained on plume centerline using cylindrical probes of various length to diameter ratios were consistent and agreed well with the data obtained using a spherical probe of 0.32 cm (0.125 in) diameter. The electron density was found to be proportional to the inverse distance squared for the entire range investigated (i.e. up to 3 cm). In the near field the radial decay of the electron density from the centerline peak followed neither a cosine nor an exponential distribution as presented in other source flow models.

Comparison of the data obtained by this study with the electron density data previously obtained in the nozzle and plume indicated that the source flow approximation appeared to break down in the region less than 3 cm from the nozzle exit. The ion streamline data demonstrated an abrupt expansion in that region, which also indicated the breakdown of the point source model. The abrupt expansion of the flow near the nozzle may demonstrate the existence of viscous loss mechanisms in the nozzle. Further investigation of the effects of nozzle area ratio on the degree of expansion will be necessary to better understand the phenomena.

As in previous studies, an increase in thruster power level increased the electron number density throughout the plume. Some backflow of electrons was noted, but the measured electron densities were very low, nominally 2×10^{9} cm^{-3}, at radial locations immediately behind the nozzle exit.

Data obtained from the segmented anode thruster showed that an increase in electron number density results when the current attachment is forced to the farthest downstream nozzle section. Other electrical configurations did not result in changes in density.

The electron density on centerline was found to be highly dependent on the propellant mass flow rate. An increase in propellant flow resulted in a significant increase in electrons on plume centerline. This was probably due to a combination of two factors. The higher flow rate results in a higher pressure which both constricts the arc and forces the attachment point farther downstream. Greater constriction of the arc results in a higher centerline enthalpy and higher electron density. The segmented anode/nozzle data have shown that forcing the arc attachment farther downstream results in a increase in electron density on centerline.

Clearly, a great deal more work needs to be done to understand the complex physical processes occuring within the arcjet thruster. Further probe work and non-intrusive diagnostic techniques appear to be required to understand how operating parameters physically affect the performance of the arcjet.

REFERENCES

1. Wallner, L.E. and Czika, J. Jr.: "Arc-Jet Thrustor for Space Propulsion," NASA TN D-2868. June 1965.

2. Byers, D.C.: "Advanced Onboard Propulsion Benefits and Status," NASA TM 103174, July 1990.

3. Yano, S. and Knowles, S.K.: "Simulated Flight Qualification Test of an Engineering Model Arcjet System," Proceedings of the 1989 JANNAF Propulsion Meeting, Cleveland, OH, 1989.

4. Curran, F.M. and Haag, T.W.: "An Extended Life and Performance Test of a Low Power Arcjet," AIAA 88-3106, July 1988 (NASA TM-100942).

5. Zafran, S.: "Arcjet System Integration Development Program," Final Report, NASA CR-185266, TRW, Inc., Redondo Beach, CA, (to be published).

6. Carney, L.M.: "An Experimental Investigation of an Arcjet Thruster Exhaust Using Langmuir Probes," Master's Thesis, University of Toledo, NASA TM-100258, December 1988.

7. Carney, L.M. and Sankovic, J.M.: "The Effects of Arcjet Operating Condition and Constrictor Geometry on the Plasma Plume," AIAA Paper 89-2723, July 1989. (NASA TM-102284).

8. Carney, L.M.: "Evaluation of the Communications Impact of a Low Power Arcjet Thruster," AIAA Paper 88-3105, July 1988 (NASA TM-100926).

9. Ling, H., et. al.: "Reflector Performance Degradation Due to an Arcjet Plume," presented at the 1989 Antenna Applications Symposium, Monticello, IL, September, 1989.

10. Zube, D. M.: "Emission Spectroscopy Experiments in a Low Power Arcjet Nozzle," *Diplom Ingenieur* Thesis, University of Stuttgart, Stuttgart, West Germany, 1990.

11. Manzella, et. al.: "Preliminary Plume Characteristics of an Arcjet Thruster," AIAA Paper 90-2645, July 1990, (NASA TM 103241).

12. Chen, F., Electric Probes.: *Plasma Diagnostic Techniques*, R.H. Huddlestone and S.L. Leonard, eds., Academic Press, 1965.

13. Chung, P.M., Talbot, L., and Touryan, K.J.: *Electric Probes in Stationary and Flowing Plasmas: Theory and Application*, Springer-Verlag, 1975.

14. Swift, J.D. and Schwar, M.J.: *Electrical Probes for Plasma Diagnostics*, London Iliffe Books, 1970.

15. Laframboise, J.G.: "Theory of Sperical and Cylindrical Langmuir Probes in a Collisionless, Maxwellian Plasma at Rest," University of Toronto Institute for Aerospace Studies, UTIAS-100, June 1966 (NTIS AD-634596).

16. Clayden, W.A.: "Langmuir Probe Measurements in the R.A.R.D.E. Plasma Jet," Third International Symposium on Rarified Gas Dynamics, Advances in Applied Mechanics, Vol. 2, J.A. Laurmann, ed., Academic Press, 1962, pp. 435-470.

17. Sonin, A.A.: "The Behaviour of Free Molecule Cylindrical Langmuir Probes in Supersonic Flows, and Their Application to the Study of the Blunt Body Stagnation Layer," UTIAS-109, University of Toronto Institute for Aerospace Studies, August, 1965. (NTIS AD-626451).

18. Sankovic, J.M. and Jankovsky, R.S.: "An Experimental Investigation of the Effective Current Collecting Area of a Spherical Langmuir Probe in an Arcjet Thruster Exhaust", AIAA Paper 90-0073, January 1990.

19. Jakubowski, A.K.: "Effect of Angle of Incidence on the Response of Cylindrical Electrostatic Probes at Supersonic Speeds", *AIAA Journal*, Vol. 10, 1972, pp.988-995.

20. Curran, et. al.: "Performance Characterization of a Segmented Anode Arcjet Thruster", AIAA Paper 90-2582, July 1990.

21. Haag, T.W. and Curran, F.M. : "Arcjet Starting Reliability: A Multistart Test," AIAA Paper 87-1061, May 1987, (NASA TM 89867).

22. Gruber, R.P.: "Power Electronics for a 1-Kilowatt Arcjet Thruster," AIAA Paper 86-1507, June 1986, (NASA TM 87340).

23. Simons, G.A.: "Effect of Nozzle Boudary Layers on Rocket Exhaust Plumes," AIAA Journal, Vol. 10, No.11, Sept. 1972, pp. 205-208.

24. Private Communication, Dr. Francis M. Curran, NASA Lewis Research Center, Cleveland, OH, August 1990.

Table I. Electrical configurations related to nozzle segments (1- conducting; 0- isolated)

	Segment				
	1	2	3	4	5
Configuration 0	1	1	1	1	1
Configuration 1	0	1	1	1	1
Configuration 2	1	1	1	1	0
Configuration 3	0	0	0	0	1

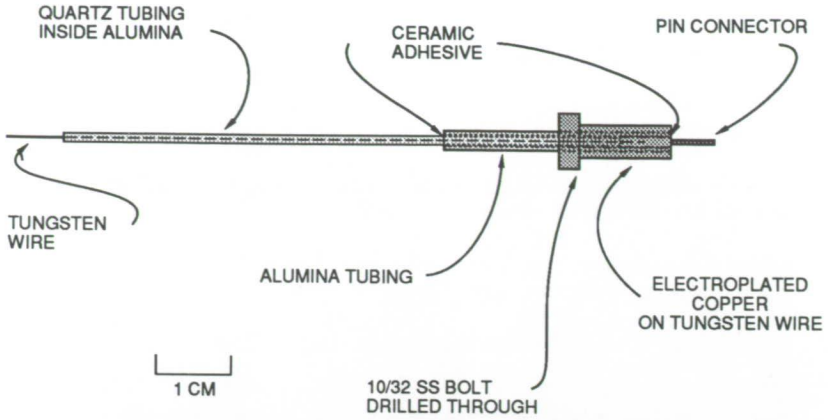

Figure 1. Typical cylindrical Langmuir probe

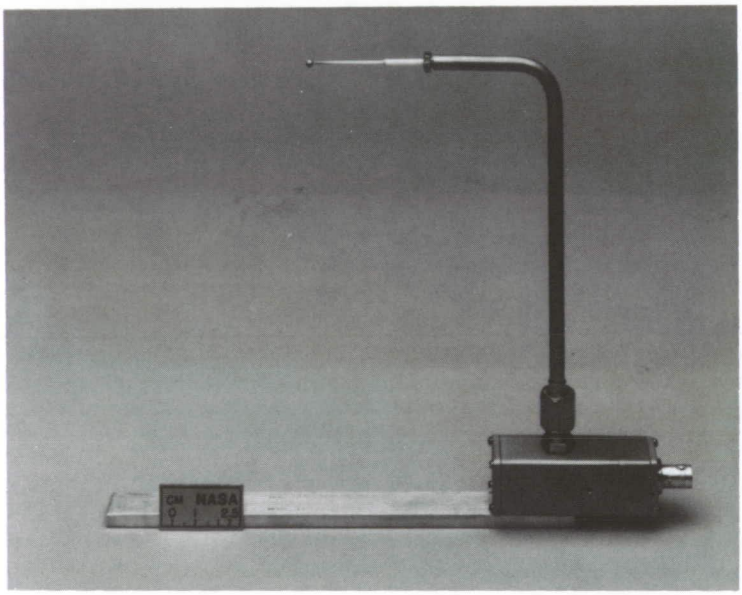

Figure 2. Spherical probe and probe support structure

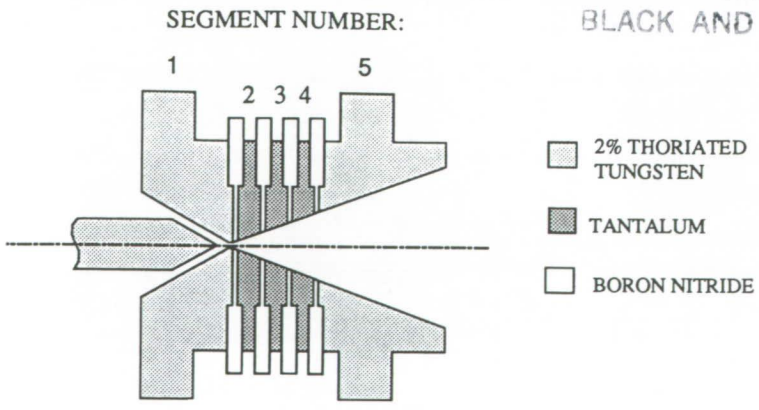

Figure 3. Thruster B anode/nozzle schematic

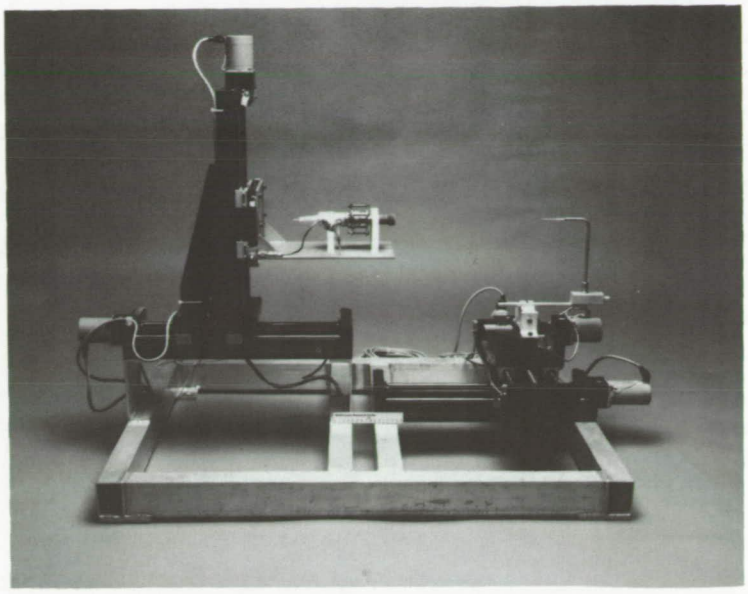

Figure 4. Arcjet and probe positioning system

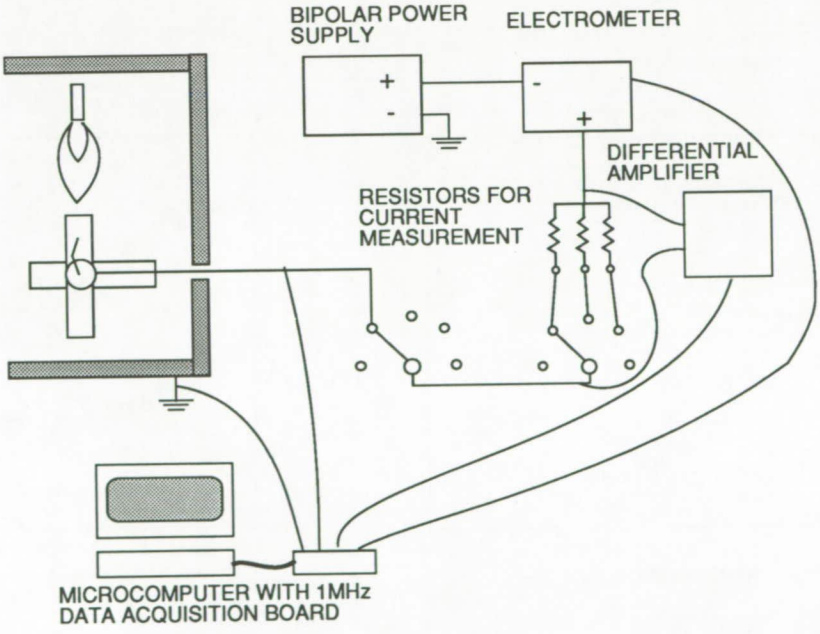

Figure 5. Schematic of experimental set-up

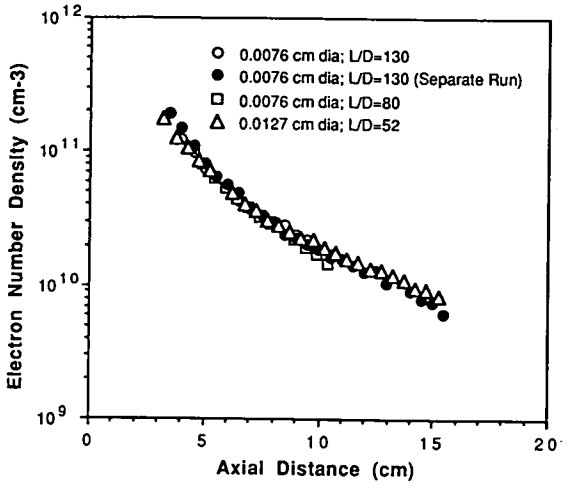

Figure 6. Electron number density as a function of axial distance for various cylindrical probe geometries. Arcjet Thruster A at 10A 115V with 1:2 N_2/H_2 flow rate of 49 mg/s.

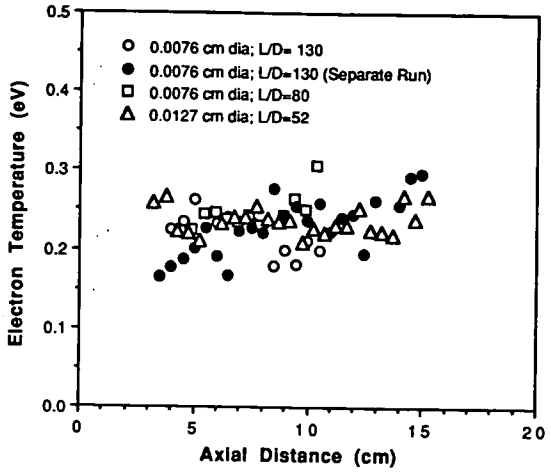

Figure 7. Electron temperature as a function of axial distance for various cylindrical probe geometries. Arcjet Thruster A at 10A 115V with 1:2 N_2/H_2 flow rate of 49 mg/s.

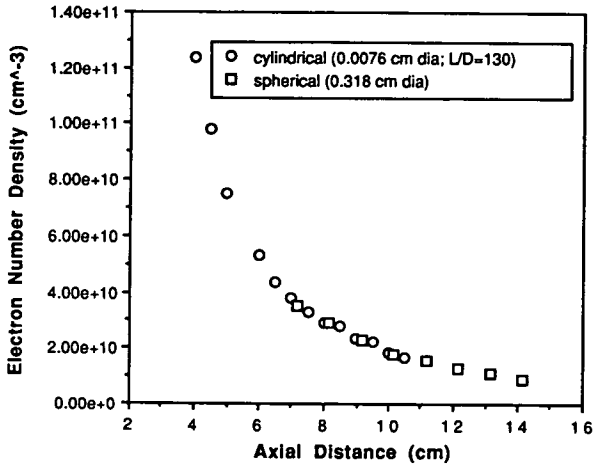

Figure 8. Electron number density as a function of axial distance for cylindrical ($1.5 \leq R_p/\lambda_d \leq 3.8$) and spherical ($53 \leq R_p/\lambda_d \leq 94$) probe geometries. Arcjet Thruster A at 10A 115V with 1:2 N_2/H_2 flow rate of 49 mg/s.

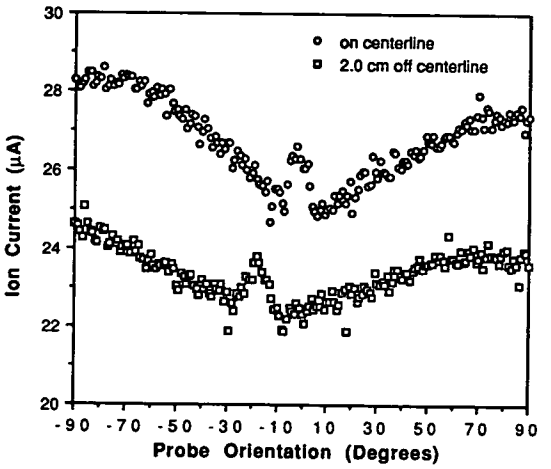

Figure 9. Ion current as a function of probe orientation at an axial distance of 8 cm. Arcjet Thruster A at 10A 115V with 1:2 N_2/H_2 flow rate of 49 mg/s.

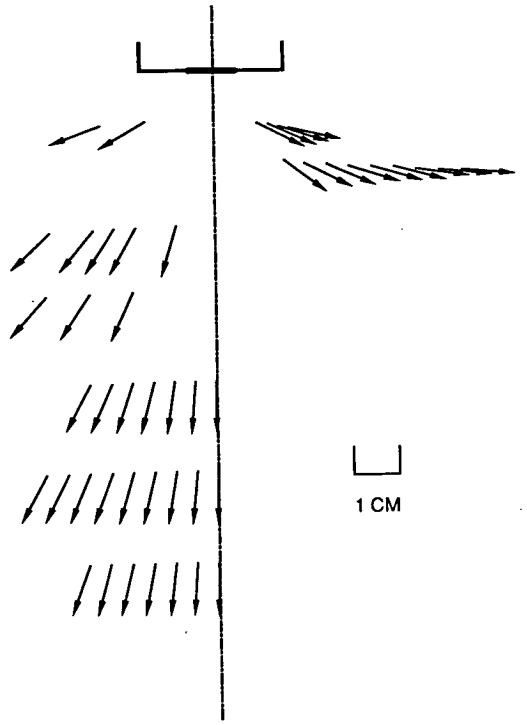

Figure 10. Ion streamlines. Arrows mark locations of data surveys. Arcjet Thruster A at 10A 115V with 1:2 N_2/H_2 flow rate of 49 mg/s.

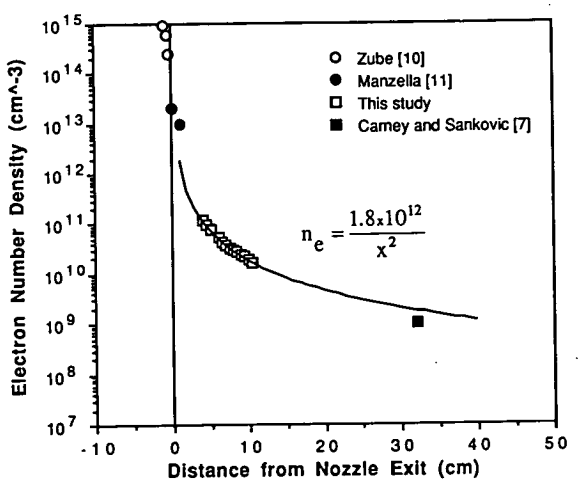

Figure 11. Electron number density at various axial distances on centerline. Comparsion of data obtained in this study with previous data for other regions of the plume.

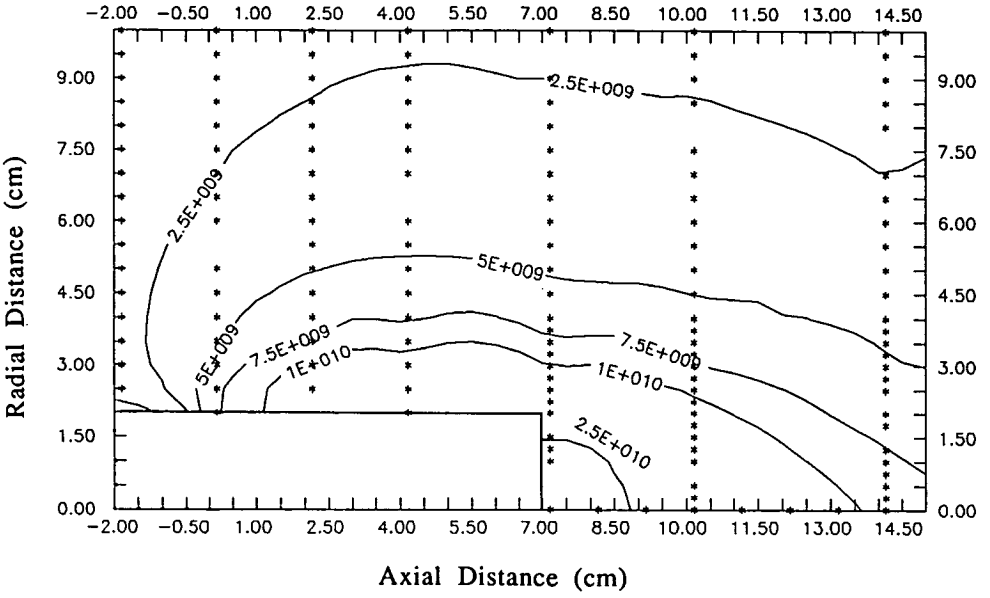

Figure 12. Electron density contour for Thruster A at 1140 W 10A with 1:2 N_2/H_2 flow rate of 49 mg/s. Zero axial distance corresponds to nozzle exit plane. All density values in cm^{-3}.

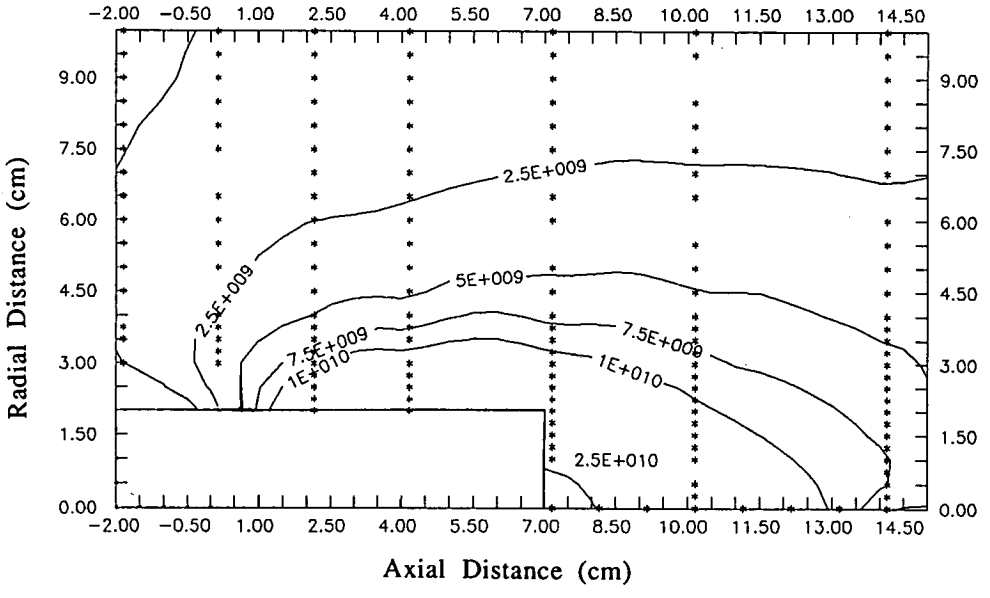

Figure 13. Electron density contour for Thruster A at 940 W 7.5A with 1:2 N_2/H_2 flow rate of 49 mg/s. Zero axial distance corresponds to nozzle exit plane. All density values in cm^{-3}.

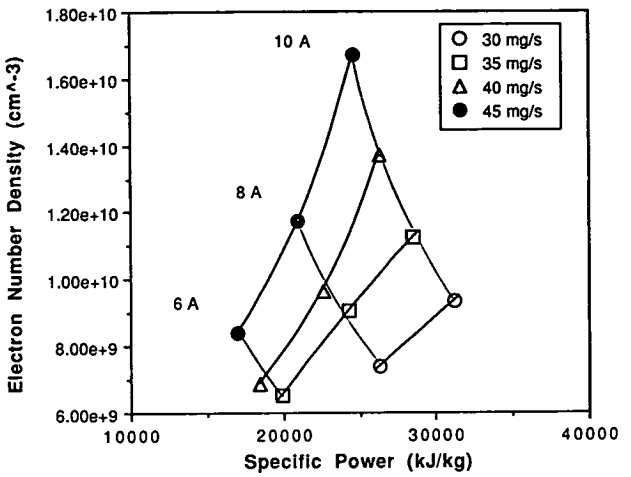

Figure 14. Electron density as a function of specific power at constant current levels and constant propellent mass flow rates on centerline at an axial distance of 10.16 cm for Thruster A.

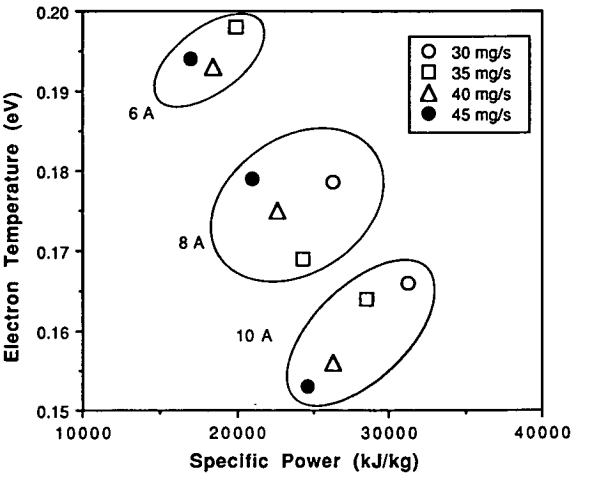

Figure 15. Electron temperature as a function of specific power at various current levels and propellent mass flow rates on centerline at an axial distance of 10.16 cm for Thruster A.

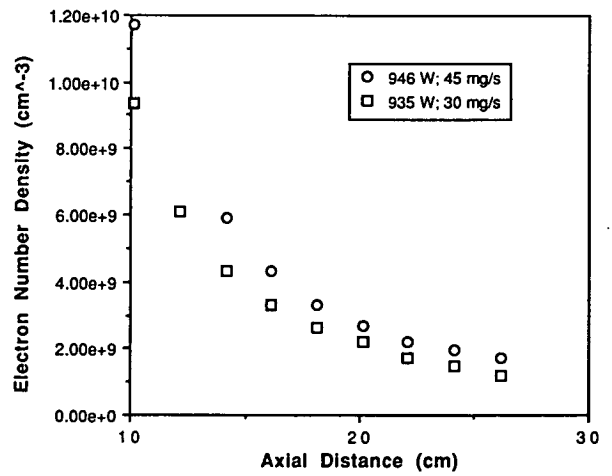

Figure 16. Electron number density as a function of axial distance on centerline for Thruster A at 940W and various propellant flow rates.

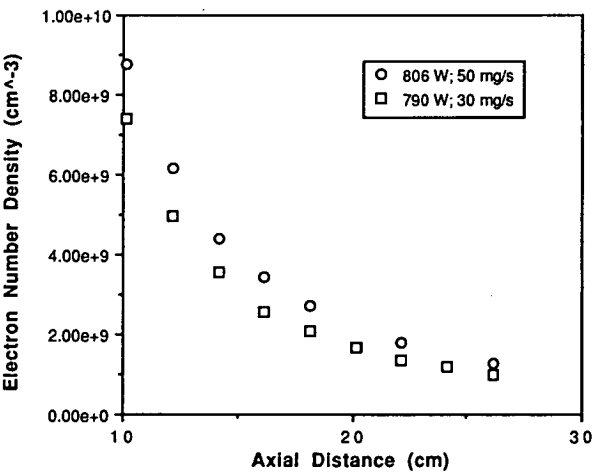

Figure 17. Electron number density as a function of axial distance on centerline for Thruster A at 800W and various propellant flow rates.

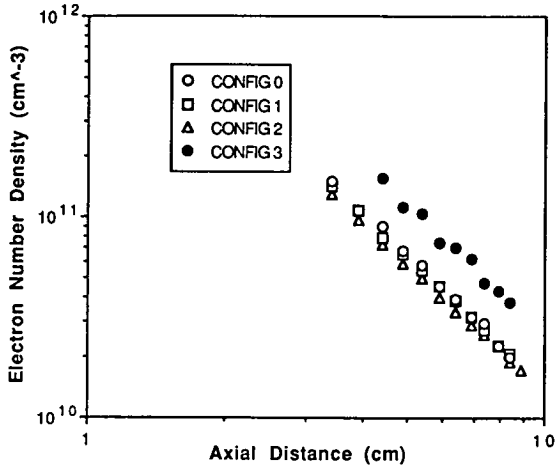

Figure 18. Electron number density as a function of axial distance on centerline at electrical configurations for Thruster B at 10A and a 1:2 N_2/H_2 propellant flow rate of 49 mg/s.

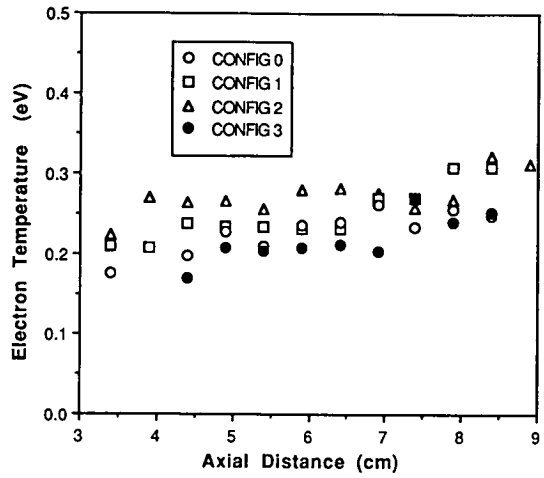

Figure 19. Electron temperature as a function of axial distance on centerline at various electrical configurations for Thruster B at 10A and a 1:2 N_2/H_2 propellant flow rate of 49 mg/s.

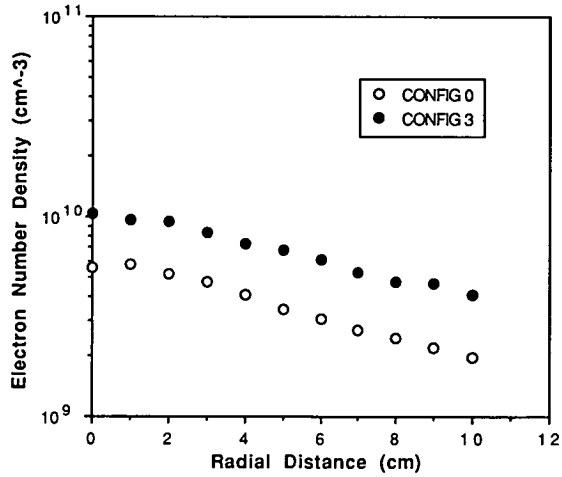

Figure 20. Electron number density as a function of radial distance at an axial distance of 14.16 cm for Configurations 0 and 3. Thruster B at 10A and a 1:2 N_2/H_2 propellant flow rate of 49 mg/s.